Materials Today Bio 28 (2024) 101219

Contents lists available at ScienceDirect

Materials Today Bio

journal homepage: www.journals.elsevier.com/materials-today-bio

Injectable polypeptide-polysaccharide depot for preventing postoperative tumor recurrence by concurrent *in situ* chemotherapy and brachytherapy

Jiaming Fan [a,b,1], Xiaoyao Cai [c,1], Han Gui [c], Lin Mei [d], Wei Xu [e], Dianyu Wang [c], Youtian Zhang [a,b], Chen Gao [a,b], Lijun Yang [c], Cuihong Yang [c], Jinjian Liu [c,**], Yong Guan [b,***], Jianfeng Liu [c,*]

[a] *Tianjin Medical University, Tianjin, 300070, PR China*
[b] *Department of Urology, Tianjin Children's Hospital/Tianjin University Children's Hospital, Tianjin, 300134, PR China*
[c] *State Key Laboratory of Advanced Medical Materials and Devices, Tianjin Key Laboratory of Radiation Medicine and Molecular Nuclear Medicine, Key Laboratory of Radiopharmacokinetics for Innovative Drugs, Tianjin Institutes of Health Science, Institute of Radiation Medicine, Chinese Academy of Medical Sciences & Peking Union Medical College, Tianjin, 300192, PR China*
[d] *State Key Laboratory of Advanced Medical Materials and Devices, Tianjin Key Laboratory of Biomedical Materials, Key Laboratory of Biomaterials and Nanotechnology for Cancer Immunotherapy, Institute of Biomedical Engineering, Chinese Academy of Medical Sciences and Peking Union Medical College, Tianjin, 300192, PR China*
[e] *Department of Pathology, Characteristic Medical Center of Chinese People's Armed Police Forces, Tianjin, 300180, PR China*

ARTICLE INFO

Keywords:
Polypeptide-polysaccharide
Postoperative tumor recurrence
Depot hydrogels
Chemotherapy
Brachytherapy
Vincristine

ABSTRACT

Chemotherapy and radiotherapy in combination with sequence regimens are recognized as the current major strategy for suppressing postoperative tumor recurrence. However, systemic side effects and poor in-field cooperation of the two therapies seriously impair the therapeutic efficacy of patients. The combination of brachytherapy and chemotherapy through innovative biomaterials has proven to be an important strategy to achieve synergistic effects of radiotherapy and chemotherapy in-time and in-field. However, for postoperative chemoradiotherapy, as far as we know, there are few relevant reports. Herein, an injectable pH-responsive polypeptide-polysaccharide depot for concurrent *in situ* chemotherapy and brachytherapy was developed by encapsulating vincristine into iodine-125 radionuclide labeled hydrogel. This depot hydrogel was prepared by dynamic covalent bonds of Schiff base between aldehydeated hyaluronic acid and polyethylene glycol-polytyrosine. Therefore, this hydrogel enables smart response to tumor acidic microenvironment, rapid release of the encapsulated vincristine and an enhanced uptake effect by tumor cells, which significantly reduces IC_{50} of vincristine for the anaplasia Wilms' tumor cells *in vitro*. This depot hydrogel shows excellent stability and biocompatibility, and maintains for 14 days after *in situ* injection in a postoperative model of anaplasia Wilms' tumor. After injection at the cavity of tumor excision, responsively-released vincristine and the radioactive iodine-125 exerted excellent killing effects on residual tumor cells, inhibiting tumor relapse and liver metastasis of the recurrent tumor. Hence, this study proposes an effective therapeutic strategy for inhibiting anaplasia Wilms' tumor recurrence, which provides a new approach for concurrent postoperative chemo-radiotherapy and a desirable guidance in regimen execution of pediatric refractory tumors.

1. Introduction

Cancer is a severe threat to human health world widely due to its high incidence and mortality. Surgery serves as the mainstay means for eliminating early-stage tumor burden, saving the life of patients [1]. However, local cancer recurrence and distant metastasis often occur in numerous malignant tumors upon surgical resection, leading to bleak prognosis and even death [1,2]. Anaplasia Wilms' tumor (AWT), a

* Corresponding author.
** Corresponding author.
*** Corresponding author.
E-mail addresses: liujinjian@irm-cams.ac.cn (J. Liu), guanyongyisheng@163.com (Y. Guan), liujianfeng@irm-cams.ac.cn (J. Liu).
[1] These authors contributed equally to this work.

https://doi.org/10.1016/j.mtbio.2024.101219
Received 6 May 2024; Received in revised form 4 August 2024; Accepted 25 August 2024
Available online 27 August 2024

subtype of Wilms tumor (WT), is characterized by high recurrence and invasiveness [3]. AWT exhibits the highest incidence of short-term recurrence (<1 year) with a survival rate less than 60 % after tumor recurrence [4]. Currently, adjuvant treatments, including chemotherapy, radiotherapy, immunotherapy and targeted therapy, are integral strategies for alleviating postoperative tumor relapse and metastasis [5–7]. In the clinical practice, combination of chemotherapy and radiotherapy has become a standard postoperative adjuvant therapy for AWT. It has long been acknowledged that chemotherapy and radiotherapy exert synergism on combating various types of tumors. For example, vincristine (VCR), the first-line chemotherapy agent, is able to arrest tumor cells in the mitotic G2/M phase by microtubule polymerization blocking effect [8]. Since DNA in G2/M phase are more likely to be damaged by ionizing radiation, chemotherapy agents like vincristine significantly sensitize radiotherapy [9]. However, problems arisen from current clinical chemo-radiotherapy regimen remain unresolved. According to clinical radiotherapy guideline of AWT, post-operative semi-abdominal irradiation is the necessary and irreplaceable treatment for lowering the risk of relapse [10]. Due to the wide irradiated area, injury on adjacent organs is inevitable [11,12]. It has recently been reported that more than 95 % of pediatric cancer survivors who have ever received semi-abdominal radiotherapy would suffer severe health problems by the age of 45, and approximately one-third would experience serious and even life-threatening chronic health problems [13]. Furthermore, most conventional chemotherapy requires high-dose and frequent administration of cytotoxic agents owing to the lack of targeting and low bioavailability, leading to serious hepatotoxicity and nephrotoxicity [14,15]. More importantly, it is difficult to achieve accurate locoregional control (i.e. in-field cooperation) over chemotherapy and radiotherapy since the short half-life of chemotherapeutic agents, potentially attenuating synergistic efficiency of chemo-radiotherapy. Therefore, it is imperative to develop a novel postoperative treatment strategy with supra-additive effects between chemotherapy and radiotherapy [16].

Hydrogels, such as polysaccharide-, peptide- and polymer-based hydrogels, have attracted substantial attention in the field of drug delivery on account of their high bioavailability, responsive release and high load efficiency of drugs, etc [17–19]. Since *in situ* injectable hydrogel has excellent shape adaptability to the irregular postoperative cavity, it has been increasingly valued for brachytherapy [20–22]. In contrast to external beam radiation therapy, brachytherapy, which is performed by tiny devices such as wires, seeds, or rods filled with radioactive materials, enables a high-dose treatment of tumor and spares surrounding normal tissues from injuries. Hydrogels loaded with radioisotopes, such as PEG-based hydrogel, have been used as medium for brachytherapy [23]. Notably, RadioGel™, which has been awarded "Breakthrough Device Designation" by FDA, is a hydrogel containing Yttrium-90 (^{90}Y) phosphate microparticles for radioisotope precision therapy. RadioGel™ will gel within the tumor interstitial spaces after injection to keep the radiation sources safely in place [24]. Besides, hydrogels can also encapsulate other therapeutic agents for targeted therapy, immunotherapy and chemotherapy, achieving combination therapy [25,26]. Remarkably, injectable hydrogels are the most suitable depots for in-field cooperation of brachytherapy and chemotherapy [17]. Through reasonable design, the supra-additive effect of brachytherapy and chemotherapy can be achieved with minimum synergistic toxicities [27–29]. However, studies of hydrogel co-loaded with chemotherapy and brachytherapy for postoperative tumor treatment are still rarely reported. Therefore, developing an injectable hydrogel loaded radioisotope and chemotherapeutic agent will pave the way for the future application of postoperative concurrent chemotherapy and brachytherapy.

Herein, we designed and fabricated a polypeptide-polysaccharide depot hydrogel (named as VCR@HPPY(^{125}I) for preventing postoperative tumor recurrence by concurrent *in situ* chemotherapy and brachytherapy (Scheme 1). The hydrogel was formed by crosslink

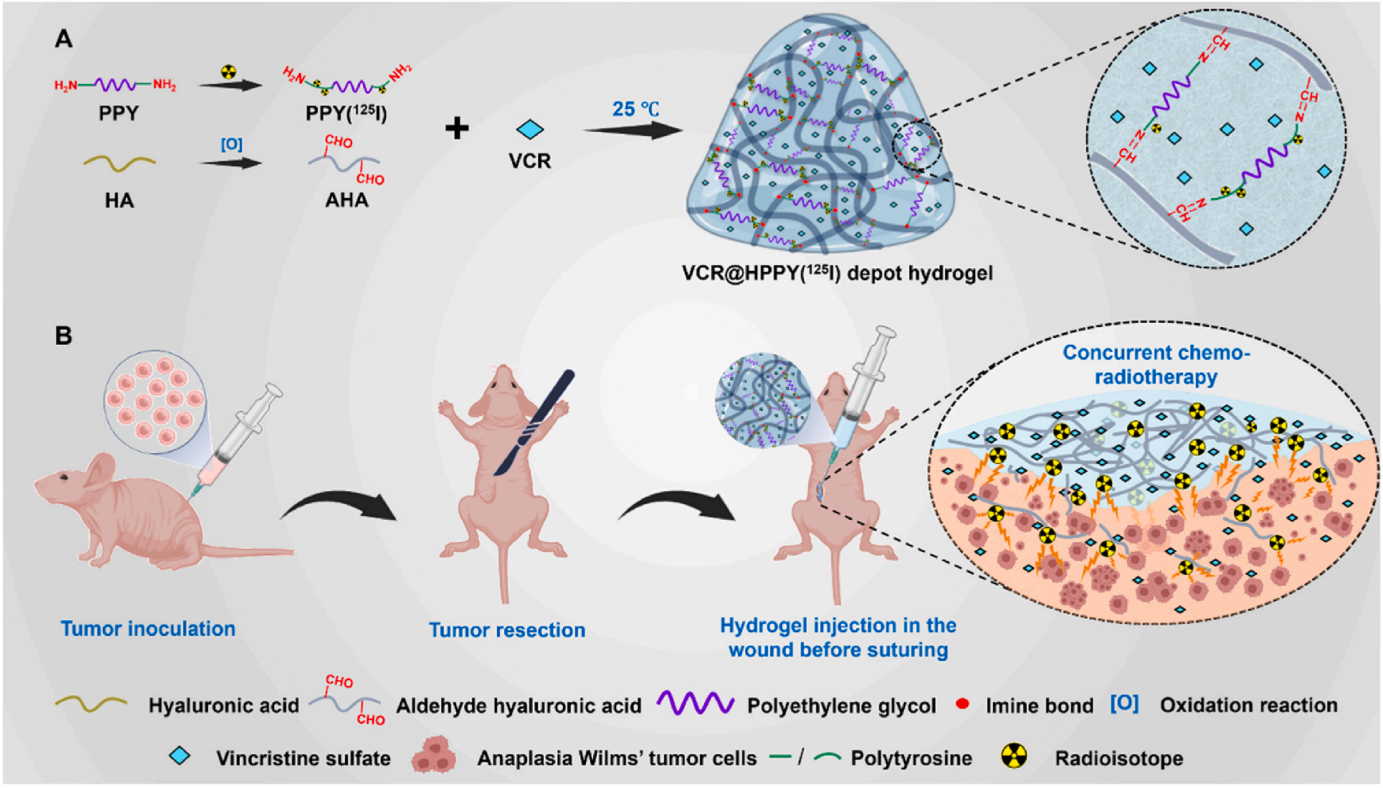

Scheme 1. Schematic illustration of (A) the preparation of VCR@HPPY(^{125}I) depot hydrogel and (B) its application in postoperative concurrent *in situ* chemotherapy and brachytherapy for anaplasia Wilms' tumor.

between aldehydeated hyaluronic acid (AHA) and polyethylene glycol-polytyrosine (PEG-PTyr) *via* Schiff base reaction, which served as a pH triggered depot for cytotoxic agent VCR and conjugated radioisotope iodine-125 (^{125}I). The released vincristine not only acted as a direct killing agent for inhibiting the division and proliferation of tumor cell, but also significantly strengthened brachytherapy. VCR@HPPY(^{125}I) showed excellent stability and biocompatibility, and could be retained in the resection site of AWT for 14 days, allowing an efficient depot for both chemotherapy and brachytherapy. *In vivo* experiments showed that the pH-responsive release of VCR and brachytherapy with ^{125}I could synergistically reduce AWT recurrence rate. Moreover, it could also inhibit liver metastasis of postoperative recurrent tumor. This strategy of employing *in situ* injectable and bio-responsive hydrogel for concurrent chemo-radiotherapy provided a new approach with supra-additive effect and minimum toxicities for postoperative management of refractory tumors.

2. Materials and methods

2.1. Materials

Diamino polyethylene glycol (NH_2-PEG-NH_2, Mw = 5 kd) was purchased from Fluka Corporation. L-tyrosine-N-carboxyanhydride (Tyr-NCA) and indocyanine green (ICG) were obtained from Xi'an Ruixi Biological Technology Co. Ltd. (Xi'an, China). Iodine-125 (^{125}I) radionuclide (500 mCi mL^{-1} in 0.1m NaOH solution) was obtained from PerkinEmer Co. (USA). N,N′-dimethylformamide (DMF), dimethyl sulfoxide (DMSO), chloramine-T, sodium pyrosulfite ($Na_2S_2O_5$) and sodium periodate ($NaIO_4$) were obtained from J&K Chemical Technology Co. Ltd. (Beijing, China). Hyaluronic acid (HA, Mw = 100kd) was obtained from Heowns Biochemical Technology Co., Ltd. (Tianjin, China). Acetonitrile (99.9 %, GC) and methyl alcohol (99.9 %, GC) were obtained from Concord Technology Co. Ltd. (Tianjin, China). Triethylamine (99.5 %, GC) and acetic acid (99.5 %, AR) were purchased from Shanghai Aladdin Biochemical Technology Co., Ltd. (Shanghai, China). Vincristine sulfate (VCR, 98 %) was purchased from Shanghai Macklin Biochemical Technology Co. Ltd. (Shanghai, China). Human Wilms' Tumor (WiT49) cell line used in this work was purchased from the American Type Culture Collection (ATCC, Rockville, USA). Trypsin, penicillin/streptomycin (P/S), fetal bovine serum (FBS), Dulbecco's Modified Eagle Medium (DMEM), Cell Counting Kit-8 (CCK-8) and 4′,6-diamidino-2-phenylindole dihydrochloride (DAPI) were purchased from Gibco BRL (Eggenstein, Germany). The Calcein-AM/PI double stain kit was purchased from Yeasen Biotechnology Co. Ltd. (Shanghai, China). Annexin V apoptosis was purchased from BD Pharmingen (San Diego, CA, USA). The H&E staining kits was purchased from Solarbio Science & Technology Co., Ltd. (Beijing, China). The Anti-gamma H2AX antibody and Rabbit Anti-Mouse IgG H&L (Alexa Fluor® 488) were obtained from Abcam PLC (Cambridge, UK). Ultrapure Milli-Q water was used for all aqueous solutions. All other reagents were used as received. All mice used in this study were obtained from Beijing Vital River Laboratory Animal Technology Co., Ltd. (Beijing, China) and maintained in a specific pathogen-free environment.

2.2. Synthesis of PPY, PPY(^{125}I) and AHA

First, NH_2-PEG-NH_2 (1 g) and Tyr-NCA (1.035 g) were added into 2 mL of dried DMF. After dissolving the solids by ultrasonication, the mixture was sealed and stirred at 50 °C for 48 h. Then, all products were dialyzed in distilled water by using 1000 Mw dialysis bags for 3 days. Next, the pure products of PEG-PTyr (PPY) were obtained as a yellowish powder (140 mg) after lyophilization to remove excess solvent. PEG-PTyr (20 mg), Na^{125}I (160 μCi), and chloramine-T (0.16 μmol, 36.8 μg) were dissolved in 1 mL of PB (pH 7.4) and subsequently shaken for 30 min at room temperature. Then, $Na_2S_2O_5$ (0.24 μmol, 46.4 μg) was added to quench the reaction. Finally, PPY(^{125}I) was obtained by lyophilization.

Hyaluronic acid could be oxidized to aldehyde hyaluronic acid by $NaIO_4$. Briefly, HA (1 g) was dissolved in 100 mL distilled water. Next, 2.5 mmol $NaIO_4$ was dropwise added to the HA solution with constant stirring and the reaction was conducted in the dark at room temperature for 2 h. The reaction was terminated by the addition of 1 ml of ethylene glycol. After termination for 1 h, this mixture solution was dialyzed in distilled water for 3 days, and was eventually to obtain the product AHA (0.35 g) as a white flake by lyophilization.

2.3. Preparation of HPPY, VCR@HPPY, HPPY(^{125}I) and VCR@HPPY (^{125}I) depot hydrogels

Firstly, the above synthesized PPY and PPY(^{125}I) were dissolved as 7 % w/v in different concentrations solution of VCR (0 μM, 0.25 μM, 1.25 μM, 5 μM, 25 μM, 100 μM and 400 μM) with vortex, respectively. Then, AHA was added as 4.6 % w/v into above-mentioned mixture solutions to react for 1 h to form hydrogels at room temperature. The final concentration of VCR in the hydrogel were 0 μM, 0.25 μM, 1.25 μM, 5 μM, 25 μM, 100 μM and 400 μM, respectively. Hence, all these hydrogels were separated into four categories of materials such as HPPY, VCR@HPPY, HPPY(^{125}I) and VCR@HPPY(^{125}I).

2.4. Characterizations

2.4.1. Oxidative degree

0.33 g AHA was added into 25 mL 0.25 M hydroxylamine hydrochloride solution with stirring at 25 °C. After reacting for 24 h in the dark, the mixture solution was titrated by 0.1 M sodium hydroxide (NaOH) *via* potentiometric titrator. The consumption of NaOH is denoted as ΔV (mL). nNaOH (mol/L) represents the concentration of NaOH, ω indicates the weight of AHA, and 403.31 is the molecular weight of HA repeating units. The formula for calculating the oxidative degree (ODD) is as follows:

$$ODD\ (\%) = 0.5 \times 100 \times (\Delta V \times 0.001 \times nNaOH) / (\omega/403.31)$$

2.4.2. Structural composition and morphology

PPY was detected by the nuclear magnetic resonance spectrometer (Bruker, Germany, 300 MHz) and Gel Permeation Chromatography (GPC) (PLgel Oranginc GPC Column (10 μm Mixed-B, Org 300 × 7.8 mm) with RI2000 detector) to confirm the synthesis and composition of PPY. Functional groups on molecular structures of lyophilized AHA product was confirmed from Fourier transformed infrared spectroscopy (Perkin Elmer, USA). Lyophilized hydrogels of HPPY and VCR@HPPY were sprayed with gold and then observed *via* scanning electron microscopy (SEM) (S-4800, Hitachi) to detect the interior microstructure, respectively.

2.4.3. Rheological analysis

The rheological analysis of hydrogels was detected by using a rheometer (AR, USA). HPPY and VCR@HPPY hydrogels were coated the parallel plate at 37 °C. The elastic modulus (G′, Pa) and viscosity modulus (G'', Pa) were measured through dynamic time sweep mode using a frequency of 1 rad/s and a strain of 1 %. Viscosity (mPa·s) was detected in the range of shear rate (s^{-1}) from 0.1 to 100.

2.4.4. Radiolabeling rate and radiochemical purity

The radiolabeling rate and radiochemical purity of the fabricated HPPY(^{125}I) hydrogels were incubated with mouse plasma at 37 °C for 48 h. At the scheduled point, 10 μL of the solution was measured by a radioactive thin-layer chromatography (TLC) scanner (BioScan, AR-2000).

2.5. pH-responsive release of VCR

200 μL VCR@HPPY (200 μM) hydrogels and 400 μL PBS solutions with different pH (6.5 and 7.4) were used as the VCR release materials and medium. Mediums of different pH were added separately on the top of the hydrogel at 37 °C. At scheduled time points, 400 μL PBS solutions substituted with the same volume of PBS solutions with the corresponding pH values. All VCR release solutions from the above substitutions were harvested according to different time points and different pH values. The amount of the released VCR was measured by a High Performance Liquid Chromatograph (Waters-e2695, Waters Corp., USA) at 297 nm using methanol-acetonitrile-0.5 % triethylamine aqueous solution (20:20:60, pH = 3 adjusted with acetic acid) as the mobile phase. The concentration of VCR released at each time point is represented as C_i and the initial mass of VCR encapsulated in hydrogels is M_1. The formula for calculating the release rate (RR) is as follows:

$$RR\ (\%) = \left(0.4\sum_{i=1}^{n} C_i\right) \Big/ M_1 \times 100$$

2.6. Cytotoxicity characterization

The cytotoxicity of free drug and drug-encapsuled hydrogels were detected through a 24-well Transwell (Corning) co-culture system. Human Wilms' Tumor (WiT49) cells were seeded at the bottom of the Transwell plates (2.5×10^4 cells per well) and cultivated with 1 mL DMEM growth medium for 24 h.

2.6.1. Cell viability assay

Briefly, after the overnight seeding, medium (1 mL) with different concentration of free VCR (0 μM, 0.1 μM, 1 μM, 4 μM, 10 μM and 25 μM) or HPPY hydrogels (0 mg/mL, 5.6 mg/mL, 11.2 mg/mL, 22.4 mg/mL, 44.8 mg/mL, 89.6 mg/mL) were added to the Transwell insert chamber at 37 °C, respectively. After 24 h or 48 h of co-cultured, each medium was replaced by 1 mL medium with a 100 μL CCK8 assay to detect cell viability.

Then, 20 μL prepared VCR@HPPY hydrogels containing different amount of VCR (0 μM, 0.25 μM, 1.25 μM, 5 μM, 25 μM and 100 μM), which were equal to free VCR in 1 mL medium respectively (0 μM, 0.005 μM, 0.025 μM, 0.1 μM, 0.5 μM, 2 μM), were mixed with 1 mL medium in each upper chamber. Cell viability was evaluated using the CCK8 assay.

2.6.2. Morphology of the released hydrogel fragments

Medium (1 ml) containing free VCR (0.1 μM) and VCR@HPPY (0.1 μM VCR) hydrogel were added to the upper chamber of the above Transwell system. Subsequently, the fluid in the lower chamber was collected after 24 h and 48 h of release, respectively. Then, these liquid samples were phosphotungstic acid stained on the copper mesh for 1.5 min and dried for 12 h. The morphology of the released hydrogel fragments on the copper mesh was observed *via* the transmission electron microscope (TEM) (HT7700, Hitachi 120 KV TEM).

2.6.3. Dead-live staining assay

WiT49 cells were cultured *via* the previous Transwell co-culture system at a density of 2×10^4 cells per well, and 1 mL medium with free VCR (2 μM) and 20 μL of HPPY hydrogels and VCR@HPPY (100 μM VCR, equal to free 2 μM VCR) were added to the insert chamber at 37 °C, respectively. Normal medium with PBS treated cells were negative control. After being incubated for 24 h and 48 h, the medium was removed. Then the cells were washed twice with PBS and stained with Calcein-AM and PI solution (Calcein-AM: PI: PBS = 1:1:100) for 15 min. Finally, images of the labeled cells were captured by the confocal laser scanning microscope (CLSM, TCS SP8).

2.6.4. Apoptosis assay

WiT49 cells were cultured in the 6-well Transwell co-culture plates at a density of 2×10^5 cells per well. After the overnight seeding, 2 mL medium with free VCR (2 μM) and 80 μL of HPPY hydrogels and VCR@HPPY (50 μM VCR, equal to free 2 μM VCR in 2 mL) were added to the insert chamber at 37 °C, respectively. After being co-cultured for 24 h and 48 h, cells were all collected in tubes and given two times PBS washing. 100 μL of 1 × binding buffer was added in every tube to distribute cells. Next, 5 μL of the apoptosis detection agent of FITC-Annexin-V was added in the tubes at a room temperature and sheltered from light. After 15 min, 5 μL PI was added and continue to incubate for 15 min. Finally, 400 μL of 1 × binding buffer was loaded to each tube and mixed. Then the cell apoptosis was assessed on flow cytometry.

2.6.5. Cellular uptake detection

WiT49 cells were seeded into confocal microscopic dishes (2×10^5 cells per dish) using the complete medium and were cultured overnight. ICG was encapsulated in hydrogels as ICG@HPPY hydrogels, which was subsequently dispersed in the culture medium. Then the culture medium containing free ICG and the medium with ICG@HPPY hydrogel were treated with tumor cells. After 24-h co-culture, the cells were washed with PBS and fixed with 4 % PFA for 30 min, then washed with PBS again. Then the cell nuclei were stained with DAPI. Last, all tumor cells were captured by CLSM.

2.7. γ-H2AX detection

WiT49 cells were seeded in the laser confocal petri dish with 2×10^4 per well. Then, the HPPY, HPPY(^{125}I) and VCR@HPPY(^{125}I) hydrogels (16 μCi/20 μL) were added as described in "Cytotoxicity characterization." After being treated for 48 h, the cells were washed with PBS and fixed with 4 % PFA for 30 min, then washed with PBS again. The above cells were permeabilized the membrane with pre-cooled methanol for 15 min and blocked with 1 % BSA for 1 h. Then the cells were incubated with γ-H2AX antibodies overnight at 4 °C. After washing with PBS, the cells were incubated with secondary antibodies at room temperature for 2 h. The cell nuclei were then stained with DAPI. Finally, the γ-H2AX stained cells were captured by CLSM.

2.8. Radiolabeled retention and biosafety

2.8.1. In vivo retention of radioactive hydrogel

The fabricated HPPY(^{125}I) hydrogel were embedded in the dorsal subcutaneous tissue of female BALB/C mice (n = 3, 160 μCi/200 μL). NanoScan SPECT/CT (Mediso, USA) was used at the predetermined periods (0, 1, 3, 5, 7, 14 days) to detect distribution and strength of radioactive signals in mice. Images were captured from the prone position.

2.8.2. Biosafety of radioactive hydrogels

An automatic blood analyzer (Celltace, Japan) was used to evaluate potential hematological side effects in mice during the acute and chronic phases (1 day, 7 days and 14 days) after radioactive hydrogels administration. Mice were sacrificed and major organs (heart, liver, spleen, lung and kidney) were collected by the end of the experiments. These tissues were fixed, sectioned and stained with H&E for pathological examination, compared with PBS and HPPY hydrogel groups as negative controls.

2.8.3. Hemolysis assay of hydrogels

HPPY and VCR@HPPY hydrogels with different hydrogel concentrations (5.6 mg/mL, 11.2 mg/mL, 22.4 mg/mL, 44.8 mg/mL, 89.6 mg/mL) were individually incubated with fresh rat blood (2 % in PBS, 0.5 mL) at 37 °C for 4 h. Positive and negative controls were used using Triton X-100 and PBS, respectively. After centrifugated (3000 rpm/min)

for 10 min, the hemolysis photos were captured by camera. Subsequently, the supernatant was measured the absorbance at 570 nm to calculate the hemolysis ratio.

2.9. In vivo anti-tumor experiments

The Wilms' Tumor model was established by subcutaneously inoculating tumor cells (1×10^6 WiT49 cells in 100 μL PBS per mouse) into the right flank of female BALB/c nude mice (4–6 weeks old). WiT49 xenograft-bearing nude mice were randomly divided into six groups (5 mice per group): Control (PBS), HPPY, VCR, VCR@HPPY, HPPY(^{125}I) and VCR@HPPY(^{125}I). After inoculation, the tumor size was monitored once every two days. When the tumors grew up to 50–80 mm^3, Surgery of tumor resection were conducted after the mice were anesthetized. After suturing the wound, corresponding drugs or hydrogels (160 μCi/200 μL) were injected into the excision of the tumor site. The tumor size and body weight were monitored at predetermined time during 18 days. The formula for calculating the tumor volume (V) is as follows.

$$V = (\text{Tumor length} \times \text{Tumor width}^2) / 2$$

Mice were sacrificed when the tumor size reached 2000 mm^3. Then, the major organs (heart, liver, spleen, lung and kidney) and tumors were excised immediately and fixed in Formalin solution. Tumors were sectioned for H&E staining and TUNEL fluorescence staining. Major organs were sectioned and then stained with H&E for pathological analysis.

2.10. Statistical analysis

All data were shown as mean ± standard deviation (SD) with sample size (n = 3–6) as specified in the experiments. Statistical analysis among two groups were determined by two-sided Student's t-tests, and multiple

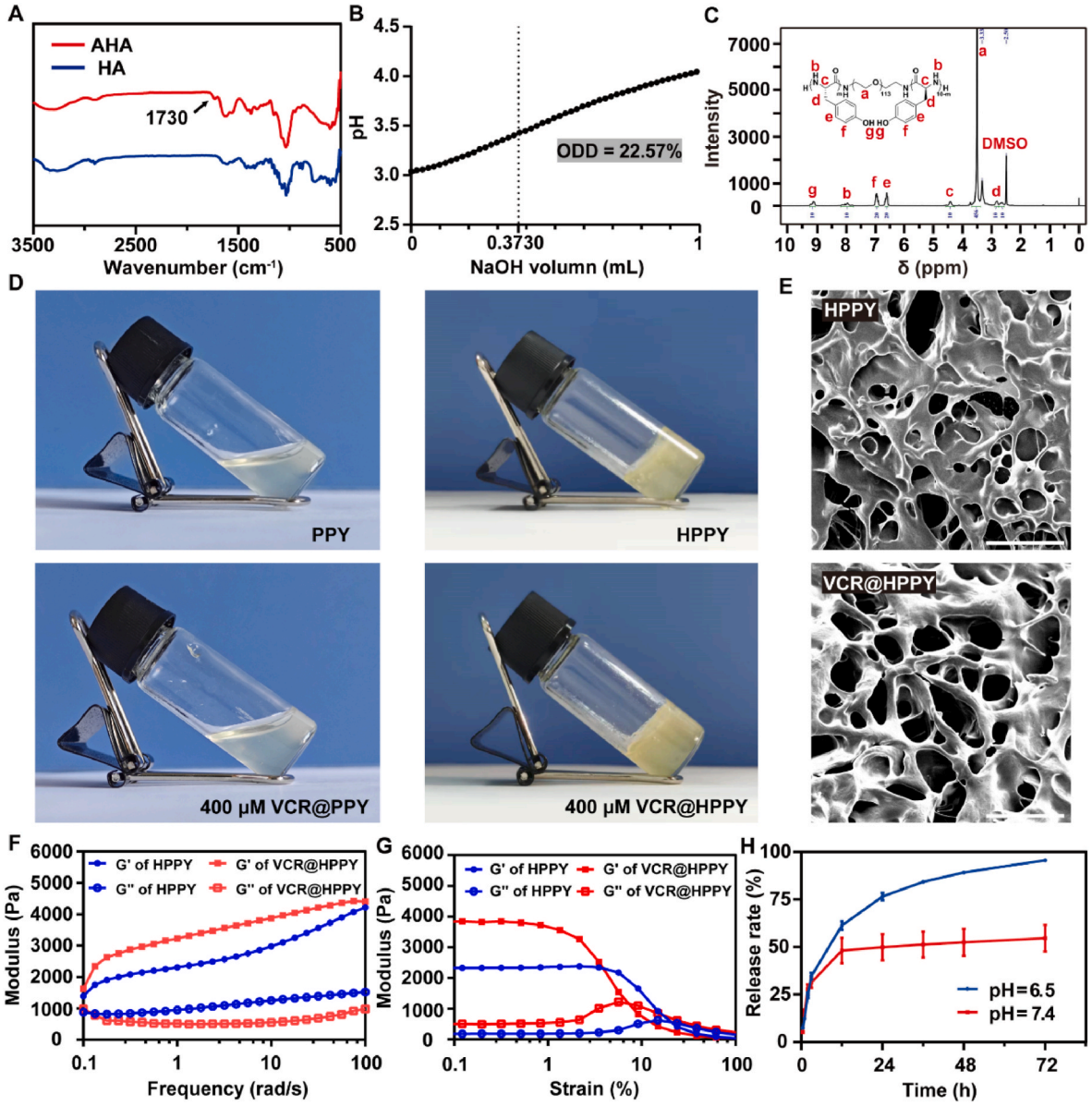

Fig. 1. Preparation and characterization of VCR@HPPY hydrogels. (A) FT-IR spectra of AHA and HA. (B) Hydroxylamine hydrochloride-potentiometric titration curve of AHA. (C) ^{1}H NMR spectrum of PPY. (D) Optical images of HPPY and VCR@HPPY (400 μM) hydrogels (PPY: AHA = 1 : 10). (E) SEM images of HPPY and VCR@HPPY hydrogels. Scale bar: 80 μm. (F–G) Rheological analysis of HPPY and VCR@HPPY hydrogels from respectively frequency sweep at 1 % strain and strain sweep at 1 rad/s frequency. (H) The VCR releasing profile of VCR@HPPY (200 μM) at different pH conditions. Data presented as the mean ± standard deviation (SD), n = 5.

groups were compared using one-way ANOVA with Tukey's post-hoc tests of Graphpad prism 8.3.0 software. Survival benefits were analyzed by using log-rank tests. p-Values below 0.05 was considered statistically significant (* for $p < 0.05$, ** for $p < 0.01$, *** for $p < 0.001$ and **** for $p < 0.0001$).

3. Results and discussion

3.1. Preparation and characterization of hydrogels

Dynamic covalent bonds maintain stable under normal conditions, but dynamic under certain stimuli, including light, temperature, and pH, etc [30]. This unique property renders hydrogel responsive drug release, adaptability and self-healing, etc. In order to form imine bonds responsive to acidic microenvironments [31], HA was oxidized to provide aldehyde group of the imine bond (Fig. S1). FT-IR spectra confirmed the generation of the aldehyde group as its peak appeared at 1730 cm^{-1} (Fig. 1A and Fig. S2). Furthermore, according to the volume of NaOH consumed at the end of the potentiometric titration of hydroxylamine hydrochloride, the oxidative degree (ODD) of AHA was calculated to be 22.57 % (Fig. 1B). The amino terminus in imine bond is contributed by FDA-approved PEG-NH_2. Considering that tyrosine (Tyr) is readily labeled with ^{125}I, Tyr is utilized to conjugated with PEG by the ring-opening polymerization reaction between Tyr-NCA and PEG-NH_2, generating PTyr-PEG-PTyr (PPY) polymer (Fig. S3). And it was characterized by H^1 NMR and GPC to confirm its synthesis and structure (Fig. 1C and Fig. S4). The peak at 3.5 ppm was methylene proton (-CH_2O-, a) of PEG. And peaks at about 8.0, 4.4, 2.8, 6.6, 7.0, and 9.1 ppm were respectively confirmed as the secondary amine proton (-HN-, b), the methenyl proton (-$COCHCH_2$-, c), the benzyl proton (-CH_2-, d), the phenyl proton (Ar-H, e), the phenyl proton (Ar-H, f), and the hydroxyl proton (-OH, g) of PTyr in the both sides of PEG. Subsequently, the ^{125}I was labeled on PPY by chloramine-T method, generating PPY (^{125}I) (Fig. S5).

Next, in order to achieve a fully crosslink during the preparation of depot hydrogel, the molar ratio of PPY to AHA was calculated to be 1:10 according to the results of oxidation degree. The PPY were dissolved into 400 μM VCR solution (7 % w/v), while dissolved into ultrapure water was served as a control. After labeled with iodine-125, PPY or PPY(^{125}I) in VCR solution was mixed with AHA based on the above 1:10 M ratio (4.6 % w/v) to form the VCR@HPPY hydrogel or VCR@HPPY(^{125}I). As shown in Fig. 1D, PPY failed to form hydrogel at room temperature. After mixing with AHA, a stable and invertible light-yellow hydrogel (HPPY) was formed. In addition, the encapsulation of VCR and ^{125}I labelling have no effects on the formation of hydrogel (Fig. 1D and S6). The microstructure of the hydrogel was observed by scanning electron microscopy (SEM). As exhibited in Fig. 1E, both hydrogels showed a similar and typically interconnected porous gel network structure at the microscopic level. These results indicate that PPY and AHA could form stable and interconnected porous depot hydrogel.

Then, the mechanical properties of HPPY and VCR@HPPY hydrogel were examined by rheological experiments at 37 °C. The results presented that HPPY and VCR@HPPY hydrogels exhibited stable gelation in different frequency sweeps variations, namely the storage modulus (G′) was invariably higher than the loss modulus (G″), demonstrating that these hydrogels were tightly cross-linked internally and possessed favorable mechanical strength (Fig. 1F). While at high strain shear, the HPPY and VCR@HPPY hydrogels displayed an obvious gel-sol transition (G'' > G′), showing the shear-thinning property of these hydrogels (Fig. 1G). Meanwhile, the viscosity of the two hydrogels decreased with the increase of shear rate under rheological analysis, which also fully demonstrated the injectable features of our hydrogels (Fig. S7). Subsequently, the pH-responsive release behavior of VCR@HPPY hydrogels were validated by the *in vitro* drug release experiments at physiological pH (pH 7.4) and acidic microenvironment pH (pH 6.5). The amount of VCR released from hydrogels was detected by HPLC (Fig. S8). Releasing curves in Fig. 1H showed that the hydrogel in acidic microenvironment was capable of the cumulative release of 89.19 ± 0.89 % at 48 h, and nearly complete release within 72 h. In contrast, the 48-h cumulative release of hydrogels at pH 7.4 was only 52.49 ± 7.13 %. These results confirm the pH response property of imine bonds in HPPY and indicate its potential application as a depot in controlled drug release.

3.2. In vitro cytotoxicity of hydrogels

In order to detect the killing abilities of VCR@HPPY and VCR@HPPY (^{125}I) hydrogel on WiT49 cells *in vitro*, the 24-well Transwell co-culture system was harnessed to simulate the process of sustained drug release as shown in Fig. 2A. After WiT49 cells incubated in the lower chamber for 24 h, the hydrogel of each group was added into the upper chamber and cell growth was detected successively at 24 h and 48 h. The cytotoxicity of the hydrogel alone (HPPY) was evaluated to detect whether it had effects on the viability of WiT49 tumor cells. After co-incubating WiT49 cells with different concentrations of HPPY hydrogel for 24 h and 48 h, results of CCK8 assay showed that cell viability of all these hydrogels was above 90 % (Fig. 2B). Likewise, mouse epithelioid fibroblasts L929 showed similar cell viability after HPPY hydrogel treatment (Fig. S9), suggesting that HPPY hydrogel is a safe drug carrier system. Subsequently, free VCR and VCR@HPPY were respectively employed to investigate their abilities to kill cancer cells. VCR is a microtubule targeting agent by arresting microtubule protein polymerization, inducing cell apoptosis. The therapeutic efficacy of VCR is also correlated with the dose and duration of administration [32,33]. Results in Fig. 2C and D showed obvious dose and duration dependent cytotoxicity of VCR against WiT49 cells. Remarkably, as shown in Fig. 2E, compared with free VCR, VCR@HPPY was observed to exert enhanced cytotoxicity to WiT49 cells within 48 h, and the IC_{50} value of VCR decreased from 0.897 (95 % CI, 0.717–1.102) μM to 0.018 (95 % CI, 0.015–0.021) μM. The subsequent results of the dead-live staining also confirmed that dead WiT49 cells (red) increased as treatment duration increased. Moreover, more proportion of dead cells in the VCR@HPPY hydrogel group were observed than that in the free VCR group for the same treatment duration (Fig. 2F and G). Flow cytometry counts similarly indicated that both VCR@HPPY and VCR induced an increase in the number of apoptotic cells with time, and that the VCR@HPPY treatment was stronger than VCR in inducing tumor cells death (Fig. 2H and I). Based on the experimental results, we speculate that the controlled release mode of VCR from VCR@HPPY and the way the drugs enter the cells may cause VCR@HPPY to show stronger cytotoxicity. Specifically, because the free small molecules of drugs enter tumor cells mainly by diffusion [34], the free VCR in the control group was quickly released from the upper chamber and exerted a relatively short-term cytotoxic effect on tumor cells. For VCR@HPPY, disassembly of hydrogel may lead to the release of the hydrogel aggregations encapsulated VCR into the cell medium. In order to verify this speculation, we used the similar Transwell test as the above cytotoxicity assay. The VCR@HPPY hydrogel was placed in the upper chamber, and the culture medium samples in the lower chamber were observed by TEM at 24 h and 48 h. TEM images in Fig. S10 showed irregularly shaped aggregations in the VCR@HPPY hydrogel group. In order to verify the hypothesis that hydrogel aggregations were taken up more by tumor cells, the indocyanine green (ICG) fluorescent molecule was used for cellular uptake assay. The ICG was encapsulated to form ICG@HPPY hydrogels. Then the free ICG and ICG@HPPY hydrogels were treated with the WiT49 cells separately. The CLSM images showed that more ICG fluorescent signal were observed in the ICG@HPPY group at 24 h after treatment (Fig. S11). These results confirmed that these aggregations could be extensively recognized and ingested by tumor cells [35], which enhanced the cellular uptake. Based on the above analysis, boosted cellular uptake of VCR may jointly lead to the enhanced cytotoxicity of VCR@HPPY.

Afterwards, the damage to tumor cells caused by radiotherapy and

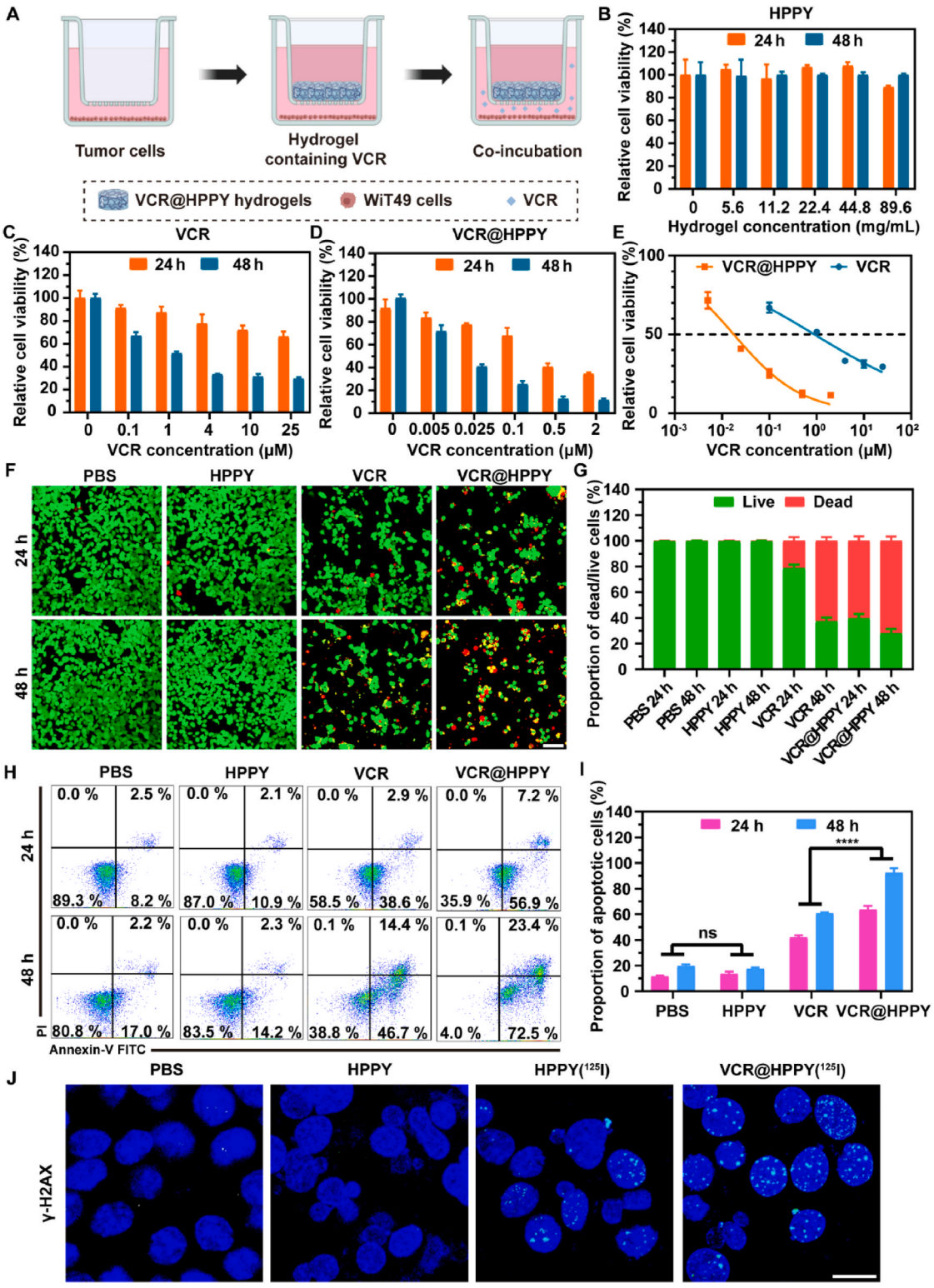

Fig. 2. *In vitro* cytotoxicity of hydrogels. (A) Schematic illustration of the tumor cells treated with the VCR@HPPY hydrogels in a Transwell co-culture system. (B) Relative cell viability of WiT49 cells after treated with different concentration of blank HPPY hydrogels for 24 and 48 h. Data presented as the mean ± standard deviation (SD), n = 3. (C) Relative cell viability of WiT49 cells after incubating with free VCR for 24 and 48 h. Data presented as the mean ± SD, n = 6. (D) Relative cell viability of WiT49 cells after treated with VCR@HPPY hydrogels containing different amount of VCR for 24 and 48 h. Data presented as the mean ± SD, n = 6. (E) The relative cell viability of WiT49 cells exposed to free VCR and VCR@HPPY respectively for 48 h with varying amount VCR concentrations: The IC_{50} values were 0.897 (95 % CI, 0.717–1.102) μM and 0.018 (95 % CI, 0.015–0.021) μM. (F–G) Representative dead-live staining images and quantitative analysis of WiT49 cells treated with PBS, HPPY, VCR and VCR@HPPY for 24 h and 48 h. Scale bar: 100 μm. Data presented as the mean ± SD, n = 3. (H–I) The representative flow cytometry plots and quantitative analysis of WiT49 cells after different treatments for 24 h and 48 h. Data presented as the mean ± SD, n = 3. (J) γ-H2AX staining images of WiT49 cells treated with blank HPPY hydrogels, HPPY(^{125}I) hydrogels and VCR@HPPY(^{125}I) hydrogels. Scale bar: 10 μm.

the combination of chemotherapy and radiotherapy were explored. ^{125}I was directly labeled to polymers PPY by chloramine-T method to form PPY(^{125}I). PPY(^{125}I) was then cross-linked with AHA at room temperature to form radioactive hydrogels HPPY(^{125}I). Afterwards, this HPPY (^{125}I) hydrogel was detected to have a radiolabeling rate of 95.04 % and its purified products showed a radiochemical purity of 100 % by TLC (Fig. S12). Ionizing radiation directly causes DNA double stranded breakages in the nucleus [36], inducing apoptosis. After DNA breakage, H2AX as histone H2A variant would be phosphorylated rapidly at Serine 139 to generate γ-H2AX [37]. Accordingly, the phosphorylated protein γ-H2AX serves to recruit DNA repair proteins. In addition, γ-H2AX also indicates double stranded breakages in a 1:1 manner, which can be harnessed as a biomarker for DNA damage. In Fig. 2G, it could be seen that evident green fluorescent signals in the nucleus were observed in

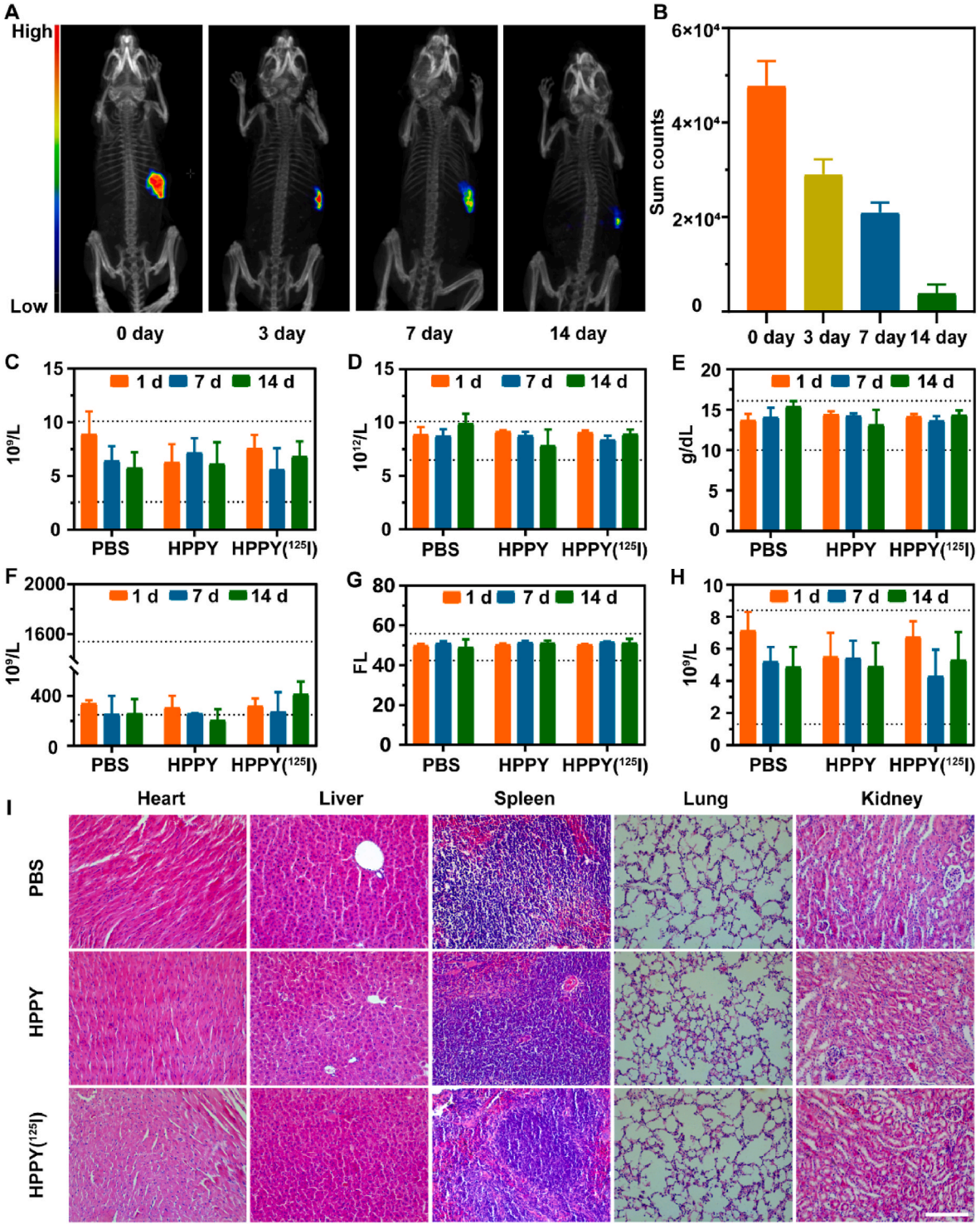

Fig. 3. *In vivo* stability and biocompatibility of HPPY(^{125}I) hydrogels. (A) *In situ* retention of the HPPY(^{125}I) depot hydrogel within 14 days. (B) The signal strength variation of HPPY(^{125}I) depot hydrogel within 14 days by SPECT. (C–H) Peripheral blood test after subcutaneous application of PBS, HPPY and HPPY(^{125}I) hydrogels: white blood cells (WBC), red blood cells (RBC), hemoglobin (HGB), platelets (PLT), mean corpuscular volume (MCV), lymphocyte ratio (LYM). Data presented as the mean ± standard deviation (SD), n = 3. (I) H&E staining of major organs after 14 days of above administration. Scale bar: 25 μm.

HPPY(^{125}I) and VCR@ HPPY(^{125}I) group, indicating that brachytherapy with radioisotopes was capable of generating DNA-damaging effects on tumor cells. Moreover, the positive signal of γ-H2AX in the VCR@HPPY (^{125}I) group, in which VCR and ^{125}I acted simultaneously, was significantly boosted compared with HPPY(^{125}I) hydrogels group, suggesting that the application of VCR could strengthen radiation-induced DNA damage. Microtubules are important cellular components for the transport of a variety of cytoplasmic proteins, including DNA damage repair proteins, to the nucleus [38]. Disruption of microtubule formation by VCR will retard the damage repair, augmenting the DNA-damaging effects of radiation on tumor cells [9]. Hence, these results demonstrated the combination treatment of VCR and brachytherapy exerts synergic killing on anaplasia Wilms' tumor cells by boosting DNA damage, laying foundation for the following *in vivo* experiments.

3.3. In vivo stability and safety of HPPY(^{125}I) hydrogel

Stabilization and biosafety of radioisotope labeling during treatment are the basis for the *in vivo* application of radioactive hydrogels. To further observe the radiochemical stability of the HPPY(^{125}I) hydrogel during treatment and determine the effective therapeutic duration of radioactive hydrogels, we continuously assayed the radiochemical purity of the HPPY(^{125}I) hydrogel incubated in mouse plasma for 14 days. As shown in Fig. S13, the HPPY(^{125}I) hydrogel still retained 99.6 % radiochemical purity by the end of 14 days. Subsequently, 200 μL of HPPY(^{125}I) hydrogel containing 160 μCi radioisotopes was injected subcutaneously into healthy BALB/C mice. The retention of the hydrogel at different time points (the 0, 1st, 3rd, 5th, 7th, 14th day) and the intensity of radioactive signal were monitored by *in vivo* SPECT imaging [39]. As shown in the SPECT-CT images of mice in Fig. 3A, the radioactive signal was mainly confined to the injection sites. Although the signal strength decreased gradually, about 10 % of the signal was still retained on the 14th day (Fig. 3B). These results suggested that HPPY (^{125}I) hydrogel is an efficient drug depot and can maintain therapeutic effects at least 14 days.

The biosafety evaluation was essential prior to the *in vivo* application of the treatment. The hemocompatibility of HPPY and VCR@HPPY hydrogels were examined by hemolysis assay. N represents the negative control group (PBS) and P refers to the positive control group (Triton X-100). Results showed that the supernatants of all hydrogel groups were clarified and the hemolysis rate of all hydrogel groups was less than 5 % (Fig. S14), which complied with the biosafety criteria. For blood tests and analysis, peripheral blood was collected on the 1st, 7th, 14th day from mice upon subcutaneous injection of HPPY(^{125}I) hydrogel, HPPY hydrogel, and PBS. Six different hematologic markers were detected, namely white blood cells (WBC), red blood cells (RBC), hemoglobin (HGB), platelets (PLT), mean corpuscular volume (MCV), and lymphocyte ratio (LYM). As shown in Fig. 3C–H and Table S1, all indicators were within normal arrange, and there were no differences among all groups, indicating that the hydrogel have no obvious adverse effects on blood system. Afterwards, the mice were sacrificed and major organs (heart, liver, spleen, lungs, and kidneys) of the mice on the 14th day of hydrogel injection were collected for pathologic analysis (Fig. 3I). The results showed that no significant pathologic changes were observed in the organs of all groups, indicating that the radioactive hydrogel treatment had a favorable biosafety.

3.4. In vivo tumor recurrence inhibition of VCR@HPPY(^{125}I) hydrogel

Encouraged by the tumor-killing ability of VCR@HPPY(^{125}I) hydrogel *in vitro* and the radiochemical stability and biocompatibility of HPPY(^{125}I) hydrogel in mice, *in vivo* inhibition of AWT recurrence was explored. For the establishment of the tumor recurrence nude mice model of AWT, 1×10^6 WiT49 cells were inoculated subcutaneously at the right flank of mice, after which the tumor was surgically removed as the volume reached 100 mm^3 (Fig. S16). Then, tumor growth at the excision site were monitored every two days, and photographs were taken to record the tumor morphology during the process of recurrence (Fig. S15). Mice showed *in situ* recurrence of tumors within 2 days after surgery, and the volume reached the physiological limit (2000 mm^3) in 14 days after surgery indicating the successful model establishment (Fig. S16).

The specific experimental process was shown in Fig. 4A. After the tumor recurrence models were established by using the above-mentioned method, the nude mice were randomly divided into six groups of PBS, HPPY, VCR, VCR@HPPY, HPPY(^{125}I), and VCR@HPPY (^{125}I). After tumor resection, treatment of each group was subcutaneously administrated into the surgically excised cavities, after which the body weights, tumor volumes, and survival of the nude mice were consistently recorded. As shown in Fig. S17, the body weights of the nude mice maintained stable for each group at the end of the study, and no significant differences were shown between the groups.

As shown in Fig. 4C, the volume of tumor in VCR group was much larger than VCR@HPPY, HPPY(^{125}I) and VCR@HPPY(^{125}I) groups, corroborating *in situ* administration of free drug alone had little capability of controlling tumor growth. The tumor size of nude mice treated with VCR@HPPY was smaller than that of VCR, suggesting that sustained release of VCR from hydrogel could obviously exert tumor inhibition effects. Notably, the tumor growth was restricted by VCR@HPPY (^{125}I) hydrogel more significantly than VCR@HPPY and HPPY(^{125}I) hydrogel groups, implying a possible synergy between chemotherapy and brachytherapy. Although studies have elucidated the synergism between vincristine and radiation, the specific synergistic mechanism needs further study [9,40]. All recurrent tumors were removed on the day 18 to measure tumor weight (Fig. 4D and E). The results show that tumor weight of VCR@HPPY (0.62 ± 0.14 g) was significantly lower than that of VCR (1.73 ± 0.70 g), corroborating that sustained release could enhance the antitumor efficacy of VCR. Furthermore, the experimental group using VCR@HPPY(^{125}I) hydrogel had the lowest tumor weight (0.06 ± 0.05 g), less than 1/10 of the tumor weight in the VCR@HPPY and HPPY(^{125}I) groups, indicative of the best therapeutic efficacy of combinatorial treatment among all groups. As shown in Fig. 4F, survival analysis within 18 days showed that the survival rates of mice treated with VCR@HPPY, HPPY(^{125}I) and VCR@HPPY(^{125}I) were all above 60 %. Further comparison revealed that the superior survival of VCR@HPPY(^{125}I) group in contrast with VCR@HPPY, HPPY (^{125}I) indicated that the combination of chemotherapy and brachytherapy is more effective in prolonging survival upon tumor recurrence (Fig. 4G). Moreover, further recurrence analysis revealed that the application of VCR@HPPY(^{125}I) depot was able to significantly delay relapse by 2–8 days versus other treatment groups (VCR@HPPY, HPPY (^{125}I), VCR groups). Notably, no significant recurrence was found in any mice of the VCR@HPPY(^{125}I) group by the 8th day after surgery in comparison to a 100 % cumulative recurrence rate in the rest of groups. This suggested that the combination of the two therapies within one depot hydrogel could be more potent in clearing the surgical residual tumor, postponing tumor recurrence, and improving the quality of survival.

Afterwards, hematoxylin and eosin (H&E) staining was conducted to observe the therapeutic effects of each treatment. Tumor in PBS, HPPY and VCR groups presented no obvious necrosis. Yet, limited areas of necrosis could be found in the VCR@HPPY, HPPY(^{125}I), and VCR@HPPY(^{125}I) hydrogel groups. Particularly, tumors in the VCR@HPPY(^{125}I) group showed massive and severe tumor necrosis and apoptosis foci, indicative of better tumor killing effects than VCR@HPPY and HPPY(^{125}I) (Fig. 5A). Subsequently, we used terminal deoxynucleotidyl transferase mediated dUTP-biotin nick end-labeling assay (TUNEL) staining to assess the ability of different treatments to induce DNA injury. As shown in Fig. 5B, VCR@HPPY(^{125}I) hydrogel induced more extensive DNA injury than HPPY(^{125}I) and VCY@HPPY did, indicating that combination treatment could aggravate DNA damages. By contrast, other groups (VCR, HPPY and PBS) triggered only minor

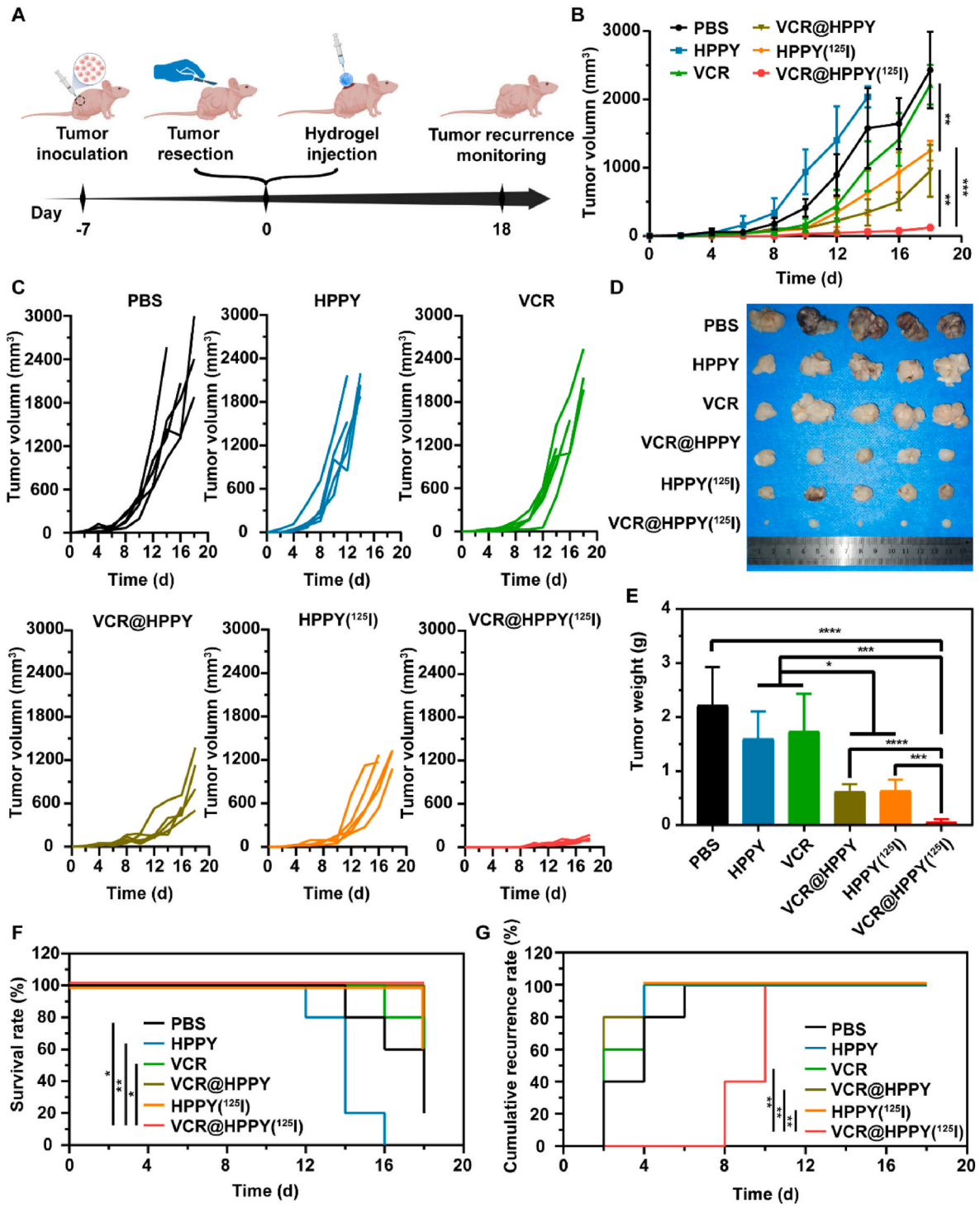

Fig. 4. Inhibition of tumor recurrence *in vivo* by depot hydrogel. (A) Schematic illustration of the establishment and treatment strategy of the WiT49 Wilms' tumor model. (B–C) Average and individual tumor volume growth profiles of BALB/c nude mice in different treatment groups. (D) Optical images of tumors after different administration on the 18th day. (E) Tumor weight of each group after various treatments. Data presented as the mean ± SD, n = 5. (F) Survival curves of BALB/c nude mice in different groups. (G) Cumulative recurrence rate of BALB/c nude mice in different groups. Data presented as the mean ± SD, n = 5. Statistical significance was calculated *via* two-sided Student's t-tests or one-way ANOVA with a Tukey post-hoc test for multiple comparisons. *p < 0.05, **p < 0.01 and ****p < 0.0001.

apoptosis, rendering difficult to inhibit the tumor recurrence. At the same time, we found the presence of white dot-like lesions in varying numbers and sizes on the surface of the livers in different groups (Fig. 5C). The livers of each group were photographed after fixed and proceeded H&E staining. It was found that none of treatments, except for the application of VCR@HPPY(^{125}I) hydrogel, were able to suppress the focal metastasis of the tumor in the liver (Fig. 5D). This was consistent with the strong tumor caused by *in situ* concurrent chemoradiotherapy, which significantly reduces the recurrence rate and inhibits the growth of recurrent tumors. This was consistent with the strong inhibition of *in situ* concurrent chemo-radiotherapy on tumor, which significantly reduced the recurrence rate and inhibited the growth of recurrent

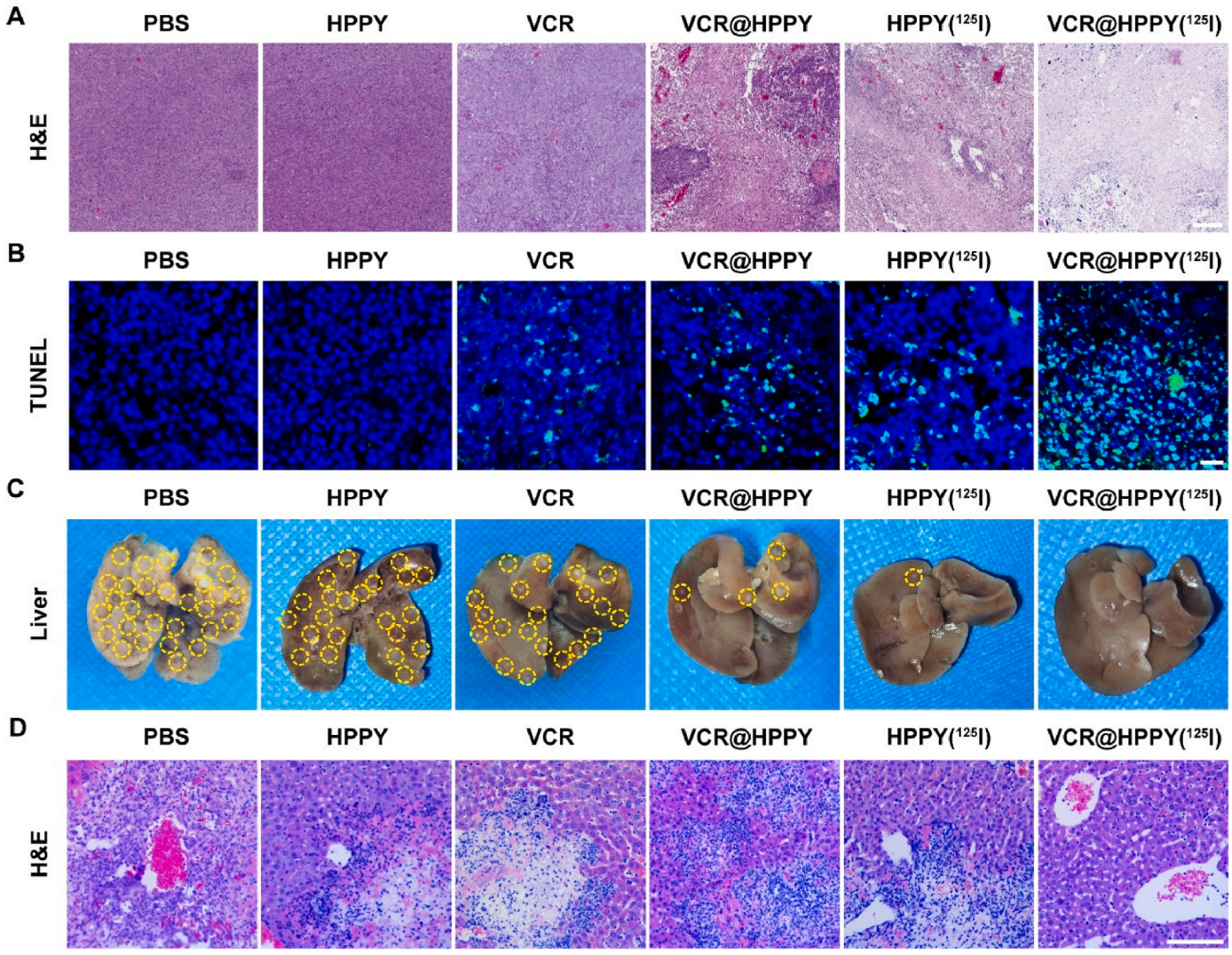

Fig. 5. Pathological analysis and inhibition of tumor liver metastases *in vivo*. (A) H&E staining of tumor tissue sections after different administration on the 18th day. Scale bar: 200 μm. (B) TUNEL and DAPI staining images of tumor tissue sections after different administration on the 18th day. Scale bar: 20 μm. (C) Optical images of tumor liver metastases BALB/c nude mice in each group. (D) H&E staining of tumor liver metastases BALB/c nude mice in each group. Scale bar: 25 μm.

tumors (Fig. 4). These results further showed that VCR@HPPY(^{125}I) hydrogel has a good potential in anti-tumor recurrence and metastasis.

4. Conclusion

In summary, we successfully designed and prepared an injectable polypeptide-polysaccharide depot loaded with vincristine and radioisotope ^{125}I, enabling the concurrent *in situ* chemotherapy and brachytherapy for inhibiting the postoperative recurrence of anaplasia Wilms' tumor. The prepared VCR@HPPY(^{125}I) hydrogel could allow for acidic pH triggered release of vincristine, exhibiting excellent tumor cells inhibition. Additionally, satisfactory biocompatibility and stability of the hydrogel guaranteed the potential of its application *in vivo*. VCR@HPPY (^{125}I) hydrogel significantly inhibited the postoperative recurrence and metastasis of the AWT tumor. Overall, our fabricated polypeptide-polysaccharide hydrogel shows an excellent depot for chemo-agents and brachytherapy radioisotopes and has great potential for application in clinical combination of chemotherapy and brachytherapy. This work establishes a novel promising platform for local concurrent postoperative chemotherapy and radiotherapy.

CRediT authorship contribution statement

Jiaming Fan: Writing – original draft, Validation, Methodology, Data curation, Conceptualization. **Xiaoyao Cai:** Writing – review & editing, Writing – original draft, Validation, Investigation. **Han Gui:** Methodology, Data curation. **Lin Mei:** Methodology, Writing – review & editing. **Wei Xu:** Methodology. **Dianyu Wang:** Software. **Youtian Zhang:** Investigation. **Chen Gao:** Methodology, Data curation. **Lijun Yang:** Software, Resources, Conceptualization. **Cuihong Yang:** Writing – review & editing, Software, Resources, Project administration, Methodology, Funding acquisition, Conceptualization. **Jinjian Liu:** Software, Resources, Methodology, Funding acquisition, Data curation. **Yong Guan:** Writing – review & editing, Supervision, Funding acquisition. **Jianfeng Liu:** Writing – review & editing, Supervision, Software, Resources, Funding acquisition, Conceptualization.

Declaration of competing interest

The authors declare that they have no known competing financial interests or personal relationships that could have appeared to influence the work reported in this paper.

Data availability

Data will be made available on request.

Acknowledgements

This work was supported by the National Key R&D Program of China (2023YFC3402800), the National Science Fund for Excellent Young Scholars (82322038), the National Natural Science Foundation of China (82172082), the Tianjin Key Medical Discipline (Specialty) Construction Project (TJYXZDXK-040A), the CAMS Innovation Fund for Medical Sciences (CIFMS 2021-I2M-1–058) and Tianjin Municipal Science and Technology Commission Grant (23ZXRKSY00010).

Appendix A. Supplementary data

Supplementary data to this article can be found online at https://doi.org/10.1016/j.mtbio.2024.101219.

References

[1] L. Wyld, R.A. Audisio, G.J. Poston, The evolution of cancer surgery and future perspectives, Nat. Rev. Clin. Oncol. 12 (2) (2015) 115–124, https://doi.org/10.1038/nrclinonc.2014.191.
[2] Y. Wu, Y. Yao, J. Zhang, H. Gui, J. Liu, J. Liu, Tumor-targeted injectable double-network hydrogel for prevention of breast cancer recurrence and wound infection via synergistic photothermal and brachytherapy, Adv. Sci. 9 (24) (2022) 2200681, https://doi.org/10.1002/advs.202200681.
[3] F. Spreafico, C.V. Fernandez, J. Brok, K. Nakata, G. Vujanic, J.I. Geller, M. Gessler, M. Maschietto, S. Behjati, A. Polanco, Wilms tumour, Nat. Rev. Dis. Primers 7 (1) (2021) 75, https://doi.org/10.1038/s41572-021-00308-8.
[4] J. Brok, M. Lopez-Yurda, H.V. Tinteren, T.D. Treger, R. Furtwängler, N. Graf, C. Bergeron, M.M. van den Heuvel-Eibrink, K. Pritchard-Jones, E. Olsen Ø, B. de Camargo, A. Verschuur, F. Spreafico, Relapse of Wilms' tumour and detection methods: a retrospective analysis of the 2001 renal tumour study group-international society of paediatric oncology Wilms' tumour protocol database, Lancet Oncol. 19 (8) (2018) 1072–1081, https://doi.org/10.1016/s1470-2045(18)30293-6.
[5] D. Kotani, E. Oki, Y. Nakamura, H. Yukami, S. Mishima, H. Bando, H. Shirasu, K. Yamazaki, J. Watanabe, M. Kotaka, Molecular residual disease and efficacy of adjuvant chemotherapy in patients with colorectal cancer, Nat. Med. 29 (1) (2023) 127–134, https://doi.org/10.1038/s41591-022-02115-4.
[6] A. Kneebone, C. Fraser-Browne, G.M. Duchesne, R. Fisher, M. Frydenberg, A. Herschtal, S.G. Williams, C. Brown, W. Delprado, A. Haworth, Adjuvant radiotherapy versus early salvage radiotherapy following radical prostatectomy (TROG 08.03/ANZUP RAVES): a randomised, controlled, phase 3, non-inferiority trial, Lancet Oncol. 21 (10) (2020) 1331–1340, https://doi.org/10.1016/S1470-2045(20)30456-3.
[7] N. Denduluri, M.R. Somerfield, M. Chavez-MacGregor, A.H. Comander, Z. Dayao, A. Eisen, R.A. Freedman, R. Gopalakrishnan, S.L. Graff, M.J. Hassett, Selection of optimal adjuvant chemotherapy and targeted therapy for early breast cancer: ASCO guideline update, J. Clin. Oncol. 39 (6) (2021) 685–693, https://doi.org/10.1200/JCO.21.02677.
[8] A. Kothari, W.N. Hittelman, T.C. Chambers, Cell cycle–dependent mechanisms underlie vincristine-induced death of primary acute lymphoblastic leukemia cells, Cancer Res. 76 (12) (2016) 3553–3561, https://doi.org/10.1158/0008-5472.CAN-15-2104.
[9] M.S. Poruchynsky, E. Komlodi-Pasztor, S. Trostel, J. Wilkerson, M. Regairaz, Y. Pommier, X. Zhang, T. Kumar Maity, R. Robey, M. Burotto, D. Sackett, U. Guha, A.T. Fojo, Microtubule-targeting agents augment the toxicity of DNA-damaging agents by disrupting intracellular trafficking of DNA repair proteins, Proc. Natl. Acad. Sci. U. S. A. 112 (5) (2015) 1571–1576, https://doi.org/10.1073/pnas.1416418112.
[10] F. Oldenburger, M.C. Cardous-Ubbink, M.M. Geenen, Evaluation of late adverse events in long-term Wilms' tumor survivors, Int. J. Radiat. Oncol. Biol. Phys. 78 (2) (2010), https://doi.org/10.1016/j.ijrobp.2009.08.016.
[11] J. Mul, E. Seravalli, M.E. Bosman, C.P. van de Ven, A.S. Littooij, M. van Grotel, M. M. van den Heuvel-Eibrink, G.O. Janssens, Estimated clinical benefit of combining highly conformal target volumes with Volumetric-Modulated Arc Therapy (VMAT) versus conventional flank irradiation in pediatric renal tumors, Clin. Transl, Radiat. Oncol. 29 (2021) 20–26, https://doi.org/10.1016/j.ctro.2021.04.007.
[12] M.J. Chen, C.R. Leao, R.C.P. Simoes, F.S. Belletti, M.L.S. Figueiredo, M.S. Cypriano, Kidney-sparing whole abdominal irradiation in Wilms tumor: potential advantages of VMAT technique, Pediatr. Blood Cancer 67 (5) (2020) e28223, https://doi.org/10.1002/pbc.28223.
[13] S. Bhatia, E.S. Tonorezos, W. Landier, Clinical care for people who survive childhood cancer: a review, JAMA 330 (12) (2023) 1175–1186, https://doi.org/10.1001/jama.2023.16875.
[14] S. Gupta, I. Portales-Castillo, A. Daher, A. Kitchlu, Conventional chemotherapy nephrotoxicity, Adv. Chronic Kidney Dis. 28 (5) (2021) 402–414.e401, https://doi.org/10.1053/j.ackd.2021.08.001.
[15] W.M.C. van den Boogaard, D.S.J. Komninos, W.P. Vermeij, Chemotherapy side-effects: not all DNA damage is equal, Cancers 14 (3) (2022), https://doi.org/10.3390/cancers14030627.
[16] K.S. Rallis, T.H. Lai Yau, M. Sideris, Chemoradiotherapy in cancer treatment: rationale and clinical applications, Anticancer Res. 41 (1) (2021) 1–7, https://doi.org/10.21873/anticanres.14746.
[17] Y. Feng, Z. Zhang, W. Tang, Y. Dai, Gel/hydrogel-based in situ biomaterial platforms for cancer postoperative treatment and recovery, Exploration 3 (5) (2023) 20220173, https://doi.org/10.1002/exp.20220173.
[18] C. Yang, G. Mu, Y. Zhang, Y. Gao, W. Zhang, J. Liu, W. Zhang, P. Li, L. Yang, Z. Yang, Supramolecular nitric oxide depot for hypoxic tumor vessel normalization and radiosensitization, Adv. Mater. 34 (37) (2022) 2202625, https://doi.org/10.1002/adma.202202625.
[19] X. Cai, W. Xu, C. Ren, L. Zhang, C. Zhang, J. Liu, C. Yang, Recent progress in quantitative analysis of self-assembled peptides, Exploration (2024) 20230064, https://doi.org/10.1002/EXP.20230064.
[20] M. Hamoudeh, M.A. Kamleh, R. Diab, H. Fessi, Radionuclides delivery systems for nuclear imaging and radiotherapy of cancer, Adv. Drug Deliv. Rev. 60 (12) (2008) 1329–1346, https://doi.org/10.1016/j.addr.2008.04.013.
[21] X. Li, X. Xu, M. Xu, Z. Geng, P. Ji, Y. Liu, Hydrogel systems for targeted cancer therapy, Front. Bioeng. Biotechnol. 11 (2023) 1140436, https://doi.org/10.3389/fbioe.2023.1140436.
[22] K. Tanderup, C. Ménard, C. Polgar, J.C. Lindegaard, C. Kirisits, R. Pötter, Advancements in brachytherapy, Adv. Drug Deliv. Rev. 109 (2017) 15–25, https://doi.org/10.1016/j.addr.2016.09.002.
[23] C. Chargari, E. Deutsch, P. Blanchard, S. Gouy, H. Martelli, F. Guérin, I. Dumas, A. Bossi, P. Morice, A.N. Viswanathan, Brachytherapy: an overview for clinicians, CA Cancer J. Clin. 69 (5) (2019) 386–401, https://doi.org/10.3322/caac.21578.
[24] D.R. Fisher, Radiation safety for yttrium-90-polymer composites (RadioGel™) in therapy of solid tumors, Health Phys. 120 (5) (2021) 510–516, https://doi.org/10.1097/hp.0000000000001369.
[25] H.F. Darge, A.T. Andrgie, H.C. Tsai, J.Y. Lai, Polysaccharide and polypeptide based injectable thermo-sensitive hydrogels for local biomedical applications, Int. J. Biol. Macromol. 133 (2019) 545–563, https://doi.org/10.1016/j.ijbiomac.2019.04.131.
[26] R. Dimatteo, N.J. Darling, T. Segura, In situ forming injectable hydrogels for drug delivery and wound repair, Adv. Drug Deliv. Rev. 127 (2018) 167–184, https://doi.org/10.1016/j.addr.2018.03.007.
[27] X. Yang, X. Chen, Y. Wang, G. Xu, L. Yu, J. Ding, Sustained release of lipophilic gemcitabine from an injectable polymeric hydrogel for synergistically enhancing tumor chemoradiotherapy, Chem. Eng. J. 396 (2020) 125320, https://doi.org/10.1016/j.cej.2020.125320.
[28] J. Liu, Y. Zhang, Q. Li, Z. Feng, P. Huang, W. Wang, J. Liu, Development of injectable thermosensitive polypeptide hydrogel as facile radioisotope and radiosensitizer hotspot for synergistic brachytherapy, Acta Biomater. 114 (2020) 133–145, https://doi.org/10.1016/j.actbio.2020.07.032.
[29] J. Yeh, B. Lehrich, C. Tran, A. Mesa, R. Baghdassarian, J. Yoshida, R. Torrey, M. Gazzaniga, A. Weinberg, S. Chalfin, J. Ravera, K. Tokita, Polyethylene glycol hydrogel rectal spacer implantation in patients with prostate cancer undergoing combination high-dose-rate brachytherapy and external beam radiotherapy, Brachytherapy 15 (3) (2016) 283–287, https://doi.org/10.1016/j.brachy.2015.12.007.
[30] F. Huang, X. Cai, X. Hou, Y. Zhang, J. Liu, L. Yang, Y. Liu, J. Liu, A dynamic covalent polymeric antimicrobial for conquering drug-resistant bacterial infection, Exploration 2 (5) (2022) 20210145, https://doi.org/10.1002/EXP.20210145.
[31] S. Bazban-Shotorbani, M.M. Hasani-Sadrabadi, A. Karkhaneh, V. Serpooshan, K. I. Jacob, A. Moshaverinia, M. Mahmoudi, Revisiting structure-property relationship of pH-responsive polymers for drug delivery applications, J. Control. Release 253 (2017) 46–63, https://doi.org/10.1016/j.jconrel.2017.02.021.
[32] B. Farasati Far, M. Omrani, M.R. Naimi Jamal, S. Javanshir, Multi-responsive chitosan-based hydrogels for controlled release of vincristine, Commun. Chem. 6 (1) (2023) 28, https://doi.org/10.1038/s42004-023-00829-1.
[33] S. Joel, The comparative clinical pharmacology of vincristine and vindesine: does vindesine offer any advantage in clinical use? Cancer Treat Rev. 21 (6) (1996) 513–525, https://doi.org/10.1016/0305-7372(95)90015-2.
[34] J. Mosquera, I. García, L.M. Liz-Marzán, Cellular uptake of nanoparticles versus small molecules: a matter of size, Acc. Chem. Res. 51 (9) (2018) 2305–2313, https://doi.org/10.1021/acs.accounts.8b00292.
[35] G. Sahay, D.Y. Alakhova, A.V. Kabanov, Endocytosis of nanomedicines, J. Control. Release. 145 (3) (2010) 182–195, https://doi.org/10.1016/j.jconrel.2010.01.036.
[36] X. Gong, B. Cui, P. Li, J. Gao, Y. Gao, X. Cai, H. Wang, W. Zhang, C. Yang, An in situ self-assembled peptide derivative for inhibition of glutathione synthesis and selective enhancement of tumor radiotherapy, iRADIOLOGY 1 (3) (2023) 199–208, https://doi.org/10.1002/ird3.31.
[37] A. Kinner, W. Wu, C. Staudt, G. Iliakis, Gamma-H2AX in recognition and signaling of DNA double-strand breaks in the context of chromatin, Nucleic Acids Res. 36 (17) (2008) 5678–5694, https://doi.org/10.1093/nar/gkn550.

[38] M. Thadani-Mulero, D.M. Nanus, P. Giannakakou, Androgen receptor on the move: boarding the microtubule expressway to the nucleus, Cancer Res. 72 (18) (2012) 4611–4615, https://doi.org/10.1158/0008-5472.Can-12-0783.
[39] J. Shi, S. Liu, Clinical application of 99mTc-labeled peptides for tumor imaging: current status and future directions, iRADIOLOGY 2 (1) (2024) 17–34, https://doi.org/10.1002/ird3.25.
[40] D. Escuin, E.R. Kline, P. Giannakakou, Both microtubule-stabilizing and microtubule-destabilizing drugs inhibit hypoxia-inducible factor-1alpha accumulation and activity by disrupting microtubule function, Cancer Res. 65 (19) (2005) 9021–9028, https://doi.org/10.1158/0008-5472.Can-04-4095.